An in-Depth Examination Modalities of Hemodynamic Characteristics in Mechanical Aortic Valve: A Comprehensive Review Article

Qabas Tariq A. Kareem[1], Samar Ali Jaber[2], Ahmed Ammar [3]

Authors affiliations:

1) Department of Biomedical Engineering, College of Engineering, Al-Nahrain University, Baghdad, Iraq.
shqabasw@gmail.com

2) Department of Biomedical Engineering, College of Engineering, Al-Nahrain University, Baghdad, Iraq
samar.a.jaber@nahrainuniv.edu.iq

3) Ibn al-Baytar Hospital, Baghdad, Iraq.
ahmed.ar.ammar@gmail.com

Abstract

The assessment of prosthetic aortic valves through echocardiography, a pivotal noninvasive tool, encounters challenges, with discordant findings compared to invasive measurements, particularly in transvalvular gradients. To address these complexities, this comprehensive review article explores diverse methodologies and modalities for assessing prosthetic aortic valve performance. As these life-saving devices advance in complexity, the demand for precise and innovative assessment techniques intensifies. This journey through established and emerging modalities aims to inform clinical practice, foster experimental innovation, and enhance patient care in the realm of aortic valve prosthetic assessment. Ultimately, a profound understanding of the hemodynamic milieu engendered by aortic prosthetic valves serves as the cornerstone for optimizing valve design and clinical utility. The primary objective of this comprehensive review is to elucidate, with utmost precision, the multifaceted methodologies employed in the investigation and evaluation of mechanical prosthetic aortic valve.

Keywords: Aortic Valve; Prosthetic Heart Valve; Biomechanics; Fluid Dynamic; Echocardiography; Computer Simulation

طرائق الفحص المتعمقة لخصائص الدورة الدموية في نماذج الصمام الأبهر الميكانيكي: مقالة مراجعة شاملة

قبس طارق عبد الكريم، سمر علي جابر، أحمد عمار

الخلاصه:

يواجه تقييم الصمام الأبهر الاصطناعي من خلال صدى القلب، وهي أداة محورية غير جراحية، تحديات، مع نتائجَ متضاربة مقارنة بقياسات التداخلات الغازية، لا سيما في التدرجات عبر الصمامات. ولمعالجة هذه التعقيدات، تستكشف مقالة المراجعة الشاملة هذه منهجيات وطرق متنوعة لتقييم أداء الصمام الأبهر الاصطناعي. ومع تقدم هذه الأجهزة المنقذة للحياة من حيث التعقيد، يتزايد الطلب على تقنيات التقييم الدقيقة والمبتكرة. تهدف هذه الرحلة من خلال الطرائق الراسخة والناشئة إلى إثراء الممارسة السريرية وتعزيز الابتكار التجريبي وتعزيز رعاية المرضى في مجال تقييم الصمام الأبهر الاصطناعي. في نهاية المطاف، فإن الفهم العميق لبيئة الدورة الدموية الناتجة عن الصمامات الاصطناعية الأبهري هو بمثابة حجر الزاوية لتحسين تصميم الصمام والفائدة السريرية

List of Abbreviation:

ALE	Arbitrary Lagrangian-Eulerian
AP	Aortic Pressure
AR	Aortic Regurgitation
AS	Aortic Stenosis
AV	Aortic Valve
BHV	Bioprosthetic Heart Valves
CFD	Computational Fluid Dynamics
CMR	Cardiac Magnetic Resonance
CO	Cardiac Output
EACTS	European Association for Cardio-Thoracic Surgery
EOA	Effective Orifice Area
ESC	European Society of Cardiology

FEM	Finite Element Method
FSI	Fluid-Structure Interaction
GOA	Geometric Orifice Area
HR	Heart Rate
LPA	Left Arterial Pressure
LVP	Left Ventricular Pressure
MG	Mean Gradients
PHV	Prosthetic Heart Valve
SAVR	Surgical Aortic Valve Replacement
SV	Stroke Volume
TR	Tricuspid Regurgitation
TRPG	Tricuspid Pressure Gradient
VTI	Velocity-Time Integral
WSS	Wall Shear Stress

1. Introduction

Within the intricate landscape of cardiac prostheses, mechanical heart valves have undergone classification, with distinctions made between one-leaflet, caged-ball, and two-leaflet valves (figure, 1). Notably, the former two have faded into obsolescence within contemporary clinical practice, giving way to the prominence of the pyrolytic carbon bi-leaflet prosthesis, which now stands as the prevailing mechanical valve of choice. While revered for its extraordinary durability, the mechanical aortic valve remains entrenched in imperfection, precluding its ascension to the status of an ideal cardiac prosthesis. A vexing dilemma in its utilization lies in the phenomenon known as prosthesis-patient mismatch, wherein the effective orifice area of the valve proves inadequate, especially within relatively larger patient anatomies. This mismatch precipitates elevated pressure gradients, leading to an augmented burden of morbidity and mortality, occasionally culminating in valve dysfunction. In the quest to comprehensively assess prosthetic aortic valves, echocardiography emerges as a ubiquitous and indispensable noninvasive imaging tool. However, despite meticulous adherence to standardized protocols championed by esteemed bodies such as the European Society of Cardiology (ESC) and the European Association for Cardio-Thoracic Surgery (EACTS), a perplexing incongruity persists. It manifests conspicuously in the form of discordant findings between echocardiographic appraisals and invasively derived metrics, most notably when quantifying trans valvular gradients across the aortic valve [1]. This stark incongruence underscores the inherent intricacy of the evaluation process; echocardiography, while invaluable in utility, occasionally falters in providing consistent, precise measurements crucial to gauging the performance of prosthetic aortic valves. This inherent variability necessitates a profound exploration of alternative or supplementary methodologies, an endeavor driven by the ultimate goal of enhancing the accuracy of assessments. Such an enhancement, in turn, holds the promise of refining patient care and ameliorating outcomes in the intricate domain of aortic valve prosthetic management. Hence, it is evident that a profound understanding of the hemodynamic milieu engendered by aortic prosthetic valves constitutes a pivotal foundation for advancing valve design and optimizing their clinical utility.

The aim of study:

The primary objective of this comprehensive review is to elucidate, with utmost precision, the multifaceted methodologies employed in the investigation and evaluation of mechanical prosthetic aortic valve.

Review outline

In the realm of hemodynamic assessment concerning mechanical aortic valve, this article is structured into six distinct sections.

First, we delve the mathematical hemodynamic derived from blood flow dynamic and pressure gradient. This encompasses: evaluation of cardiac output, the analysis of pressure gradient obtained through catheterization or Doppler measurements, the computation of effective orifice area, consideration backflow magnitude, and an exploration of various shear force types. Then, we review hydraulic simulation apparatus employed to establish controlled hemodynamic environment. Additionally, experiments involving animal models are discussed in a separated subsection. Computational investigations tool or programs have reviewed in another section that encompass modalities and methodologies related to Fluid structure interaction and multi-scale approach.

We address imaging modalities also plus examination of blood flow within the sinus proximal to the valve hinge. In the penultimate section we present a comprehensive array of clinical and experimental studies that encompass the evaluation pressure gradient parameters, effective orifice area, flow pattern and shear stresses analysis. Finally concluding notes.
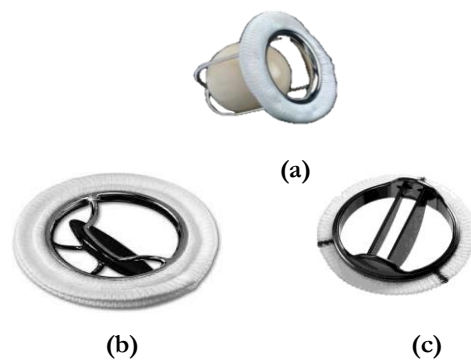

Figure (1): (a) Ball-in-cage valve, (b) monoleaflet valve, (c) Bileaflet valve [2, 3]

2 Hemodynamic assessment of prosthetic heart valve

This part reviewed the measures obtained from fluid dynamics and pressure of prosthetic heart valve.

2.1 Measures obtained from information related to fluid dynamics and pressure

In Information related to fluid dynamics and pressure include blood circulation volume from the heart, pressure gradient, effective orifice area opening area and performance index, backflow, flow configurations and forces exerted by shearing and all will reviewed in details.

2.1.1 Circulation blood volume from the heart

An effectiveness of a valve is influenced by a volume of fluid passing through it. Thus, the overall flow rate through the valve holds significant importance when evaluating its performance. The quantity of blood expelled in a single cardiac cycle is known as stroke volume (SV). Heart rate (HR) quantifies the rate at which the heart completes cycles or beats within a minute, known as beats per minute (bpm), while cardiac output (CO) indicates the quantity of blood propelled by the ventricles in each minute. Resting human heart rates range from 40 to 70 bpm, increasing to 180 to 200 bpm during physical activity. Similarly, stroke volume varies from 60 to 125 ml at rest to 100 to 200 ml during exertion. Human cardiac output ranges between 4-6 l/min and 20 to 35 l/min. The product of stroke volume (SV [ml]) and

heart rate (HR) in beats per minute yields cardiac output (CO [l/min]), as shown in equation 1[4].

$$CO = SV \cdot HR \quad \ldots\ldots..(1)$$

Changes in either stroke volume or heart rate can impact cardiac output. The computation of stroke volume involves the utilization of velocity measurements across the valve, as outlined in Equ.(2) [4].

$$SV = VTI \cdot A \quad \ldots\ldots\ldots (2)$$

Incorporating the velocity-time integral (VTI [cm]) and denoting A as the valve area in [cm2], the VTI is derived from the Doppler velocity-time graph by calculating the area beneath the velocity curve. This is expressed as $VTI = \int(R \, v \cdot dt)$.

2.1.2 Pressure gradient
The valve's opposition to the flow can be measured through the evaluation of pressure or energy losses occurring across the valve.

Pressure gradient obtained through catheterization

The dynamic systolic gradient exists between the pressures pertaining to the left ventricle and the aorta, when the pressure tracings are appropriately synchronized. It becomes feasible to ascertain the average systolic gradient, denoted as ΔP mean, by gauging a sequence of momentary pressure variances. Even if the zenith systolic pressure of the left ventricle and the aorta do not coincide in time, it remains possible to compute the gradient ΔP peak between these two peaks. It is important to note that the utmost instantaneous gradient, referred to as Pmax, consistently exceeds the peak-to-peak gradient (figure 2, a).[4]. The invasive evaluation of aortic stenosis state is still important, particularly in the following conditions: in presence of non-consistency of non-invasive measurements. valuation of certain status of aortic valve stenosis, including low-flow low-gradient state, exploration of prognostic factors influencing the procedure or clinical outcomes in Transcatheter Aortic Valve Implantation (TAVI) cases [5].
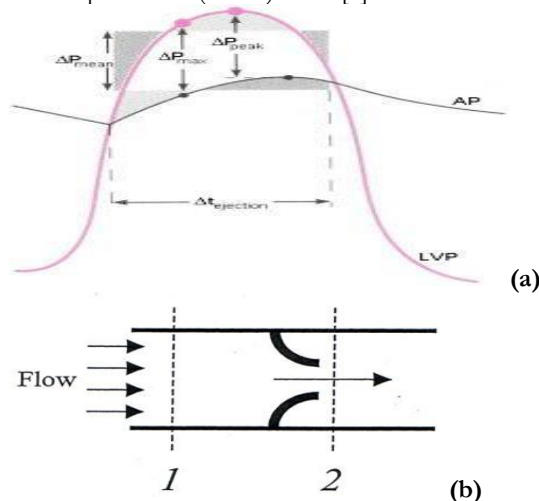

(a)

(b)

Figure (2): Pressure gradient in heart valve (a) Pressure gradient from catheterization; LVP: left ventricular pressure, AP aortic pressure. (b) Permit a narrowing to move through. The simplified Bernoulli equation is employed for approximating the variance in pressure between two points, based on evaluating the velocity at point 2 (assumed to be notably higher than at point 1) [4].

Pressure gradient from Doppler measurements

The simplified form of the Bernoulli equation is derived by assuming laminar and negligible viscous forces flow through the stenosis. Bernoulli's hydraulic equation expresses the preservation related to mechanical force interplay amid 2 locations (figure 2, b)[4].

$$P1 - P2 = \cdot \varrho(v2 - v1) + \varrho g(z2 - z1) + \varrho \int_1^2 \left(\frac{dv}{dt}\right) ds \ldots (3)$$

In relation to this formula, P1 [Pa], v1 [m/s], and z1 [m] symbolize the, force, speed and height relative to an initial point In the direction against the flow., while P2 [Pa], v2 [m/s], and z2 [m] represent the pressure, speed, and elevation at a point further downstream[4].

The simplified and modified Bernoulli equations lose accuracy when used to estimate the actual pressure gradient across a narrowed aortic valve. This limitation stems from their oversimplified assumptions involving steady, frictionless conditions, and the inherent disparities between aortic valves and idealized orifices. However, despite the availability of newer models based on time-dependent momentum balance for orifices, the simplified and modified Bernoulli equations remain the dominant choice in clinical practice. This is primarily because, as of today, they are [4]the sole models feasible for clinical implementation[6].

$$P1 - P2 = \frac{1}{2} \cdot \rho \, (v2^2 - v1^2) \quad \ldots\ldots\ldots..(4)$$

$$\Delta P \text{ Doppler [mmHg]} = 4 \cdot v2 \text{ and } v2 \text{ in [m/s]}$$

when v2 is given in meters per second (m/s) and ΔP is expressed in millimeters of mercury (mmHg)[4].

2.1.3 Effective orifice area opening area and performance index

The effective orifice area (EOA) measures the ability of a valve design to utilize its primary orifice area. This phenomenon has a particular important in the context of valve dynamics, where its maximizing of the effective valve area is crucial for reducing flow turbulence and shear stresses with the consequential notable decreases in pressure drop.
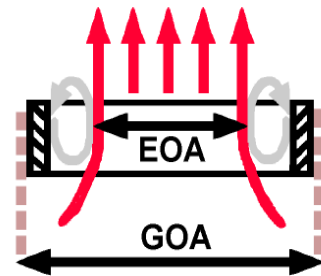

Figure (3): Orifice areas that pertain to both geometric and functional aspects (referred to as GOA and FOA, respectively)[4].

Continuity equation can estimate the EOA in [cm²] by following:

$$EOA \text{ Continuity} = SV/ VTI \quad \ldots\ldots\ldots (5)$$

Apart from the continuity equation, the Gorlin equation presents an alternate approach for computing EOA.

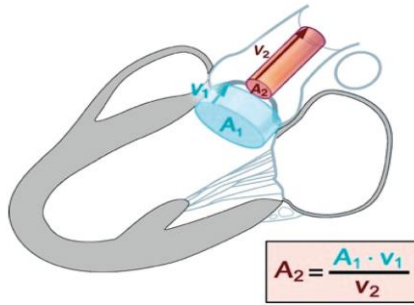
$$A_2 = \frac{A_1 \cdot v_1}{v_2}$$

Figure (4): Schematic diagram of continuity equation [7].

When considering Q as the flow rate [m³/s] with v as a highest speed [meter /second] within the point of minimum cross-sectional area, resulting in the EOA is determined using the formula [4]

$$EOA = Q / C_1 v \quad ……. (6)$$

In this situation, C_1 represents a coefficient used to adjust the velocity distribution within the point of minimum cross-sectional area (vena contracta), taking into consideration the conversion of potential energy. into kinetic energy as blood passes through the orifice. This conversion process is elucidated by[4].

$$v = C_2 . \sqrt{2. g. \Delta h} \quad …….(7)$$

Involving the pressure difference (ΔP) across the orifice and the height difference (Δz), the pressure head is represented as $\Delta h = \Delta z + \Delta P$, where in C2 stands as a coefficient (ρ g) for accommodating energy conversion losses from potential to kinetic forms. Assuming Δz is negligible (i.e., Δz = 0) and considering the condition C1•C2 = 1, parameters can be represented as[4]:

$$EOA = \frac{Q}{v} = \frac{Q}{\sqrt{2\frac{\Delta p}{\rho}}} = \frac{Q}{\sqrt{2\frac{\rho H_g \cdot g \cdot \Delta h H_g}{\rho}}} \quad …….. (8)$$

The SI units commonly employed, such as [m²], [m³/s], and [Pa], are transformed to the medical units of [cm²], [ml/s], and [mmHg] for the respective parameters of area, fluid and pressure [4].

$$EOA \ [cm^2] = 10^4 \cdot EOA \ [m^2]$$

$$Q \ [ml/s] = 10^6 . Q[m^2 /s]$$

$$\Delta P \ [mmHg] = 10^3 \cdot \Delta h_{Hg} \ [m \ Hg]$$

$$P \ Hg = 13600 \ [kg/m^3] \quad ……. (9)$$

$$g = 9.81 \ [m/s^2] \quad ……… (10)$$

Integrating equations 8 and 9 yields:

$$EOA \cdot 10^{-4} = \frac{Q \cdot 10^{-6}}{\sqrt{2 \frac{\rho_{Hg} \cdot g \cdot 10^{-3} \cdot \Delta P}{\rho}}} \quad …………(11)$$

Consequently, the Gorlin equation can be formulated as [4]:

$$EOA_{Gorlin} = \frac{Q}{51.6\sqrt{\Delta P}} \quad ……….(12)$$

Using (EOA) effective orifice area measured in [cm²], ΔP represent pressure difference indicated in [mmHg], and the mean forward flow, Q fwd mean in [ml/s] calculated as the ratio of the "positive" (associated with the forward stroke volume, SV) divided by the duration of forward flow. EOA Gorlin, is a fraction θ of the available geometric orifice area GOA, with θ known as the orifice constant, so that EOA Gorlin = θ·GOA.

Clearly a larger heart valve will have a larger EOA but may impede blood flow more compared to a small valve (depending on the valve design). In this particular case, the EOA is not a sufficient assessment for heart valve performance. This requires a normalization of heart valve size in order to compare all heart valve prostheses on equal basis. In order to do this, the performance index (PI) is defined as the ratio of the EOA to the valve geometric orifice area GOA. The PI is a quantitative measure of the effectiveness of allowing forward flow and is independent of valve size:

$$PI = \frac{EOA}{GOA} = \theta …$$

Planimetry is another common method for direct visualization of anatomic aortic valve orifice by using echocardiogram, which is better by trans-esophgeal echocardiogram. It can permit manual tracing of anatomical aortic orifice area, MRI and CT can be used also. Its tracing accuracy is questionable due to the limiting visualization in case of calcification that cause shadows or reverberations. However, aortic valve area measured by planimetry is not a primary predictor of outcome.
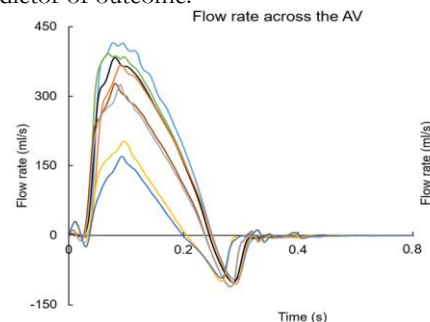
Figure(5): The flow across aortic valve: it has three components: forward movement, closing volume, and leakage volume [8].

2.1.4 Backflow flow

Regurgitation occurs when there is a backward flow through the uni-directional valve The proportion of this regurgitant per cent in regard to the overall stroke volume (SV) is determined using the following method [4]:

$$\% \ reg = \frac{V_{reg}}{(V_{reg} + SV)} \quad ………. (14)$$

The regurgitation quantity, denoted as Vreg [ml], encompasses total regurgitant volume and is able to broken down into two parts: Vclose and Vleak. Vclose pertains to the regurgitation volume linked to valve closure, while Vleak indicates the volume of regurgitation originating from the seepage of closed valve (Figure, 5) [4].

2.1.5 Flow pattern and force exerted by Shearing

Laminar and turbulent flow: Engineers can determine whether the fluid motion displays either

laminar or turbulent behavior characteristics by looking at the Reynolds number (Re; equation (15) [4].

$$Re = \rho \frac{U\,D}{\mu}$$ ……….. (15)

With p fluid density (kg/m³), U flow velocity (m/s), D vessel diameter (m), and u dynamic viscosity (mPa.s). The various flow regimes in the context of flow within a straight conduit are shown in (Figure, 6) as a function of Re. From Re = 0 to a critical value (Re 2000), at which the fluid movement in transition starts, a movement of fluid within an inflexible cylindrical conduit is typically laminar. The fluid movement in transition is fluctuating between laminar and turbulent flow (2000 < Re > 4000).
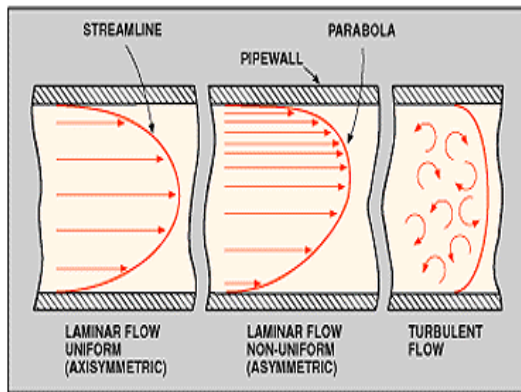

Figure (6): Laminar and turbulent flow are two types normally encountered in liquid flow Measurement operations. Most applications involve turbulent flow, with R values above 3000. Viscous liquids usually exhibit laminar flow, with R values below 2000. The transition zone between the two levels may be either laminar or turbulent[9].

When Re exceeds 3000 or 4000, the fluid flow becomes unstable. Elevated mixing leads to heightened viscous losses, which are frequently considerably greater in turbulent flow compared to laminar flow [10]. Re values as high as 4500 can be reached during peak normal aortic valve flow.

The nature of flow, whether continuous or temporary, can be established by assessing the Strouhal number. This number is given by the formula [4]:

$$Sr = \frac{D}{Tp.U}$$ ……. (16)

Here, Tp stands for the time period pertaining to the observed flow phenomena. When the Strouhal coefficient is extremely small (Sr << 1), it signifies a quasi-steady condition. On the other hand, a Strouhal number approaching one characterizes transient flow.

Shear Stresses

Blood flow applies a tangible physical pressure on the vessel wall and valve leaflet as it passes through a vessels or valves. There are two major vectors that describe this force. Shear stress, which is tangential to the wall, is a frictional force that the blood flow exerts upon the endothelium. It is called wall shear stress WSS that exerted on the surface of a blood vessel wall or a valve leaflet. Perpendicular to the wall, there is the normal stress or pressure.
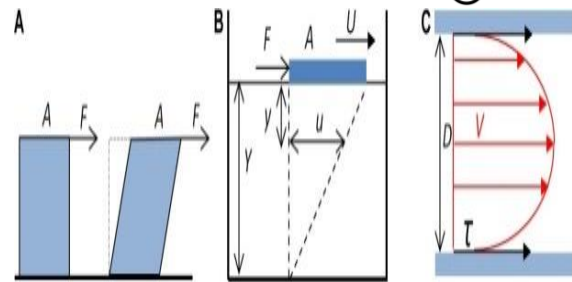

Figure (7): In essence, shear stress (A) A visual representation demonstrating shear stress, where a fluid applies a sideways force (F) to the surface area (A) of a solid (depicted as a blue cube), causing deformation in the solid. (B) Explanation of shear stress, shear rate, and viscosity. A plate (depicted as a blue block) with an area A is subjected to a lateral force (F) as it moves across the surface of a liquid with a depth Y. This movement results in displacement at the liquid's surface (U), which in turn generates fluid motion (u) at a distance y beneath the surface. The shear rate is defined as the du/dy ratio, and for a Newtonian fluid, this ratio remains constant. (C) A schematic depiction illustrating shear stress exerted by the flow of blood on the wall of a cylindrical vessel, with red arrows denoting the velocity (V) of laminar blood flow. The shear stress (τ, black arrows) exerted by the blood on the wall of the tube depends on the blood flow mean velocity, the blood viscosity, and the diameter (D) of the tube [11].

Equation 17 is employed for the calculation of shear stress in a scenario characterized by laminar flow[4].

$$\vec{\tau}_{\text{laminar}} = \mu \cdot \frac{\partial \vec{U}}{\partial y} = \mu \cdot \dot{\gamma} \qquad [\text{Pa}] \text{ or } [\text{N/m}^2]$$ … (17)

Expressing the dynamic viscosity of the fluid as μ, the velocity vector as U, and the shear rate as $\dot{\gamma}$, turbulence within the circulatory system enhances flow resistance, leading to elevated pressure differences. The calculation of turbulent shear stresses adopts a somewhat distinct method, as depicted in the provided equation18 [4].

$$\vec{\tau}_{\text{turbulent}} = \mu \cdot \frac{\partial \vec{U}}{\partial y} - \rho \overline{u'v'}$$ ………. (18)

The fluctuating turbulent velocities are denoted as u' and v'. Shear forces acting on the endothelial surface due to the flow of viscous blood continually.

Fluid shear stress is directed alterations in the gene expression pattern of endothelial cells that influence its own phenotype [12].

Platelet activation may result from high blood shear stresses resulting in thrombosis and an increased risk of embolism. At force applied parallel to a surface per unit area of 10 N/m2, blood platelet damage begins to develop. Red blood cell destruction and hemolysis also occurs at the same time as the shear stress will be greater than 200 N/m2. If there is a prolonged shear stress exposure, hemolysis may also be encountered at reduced shear stress levels values. A moving heart valve leaflet cannot be directly assessed for shear stress either in vitro or in vivo. Because of this, it is possible to estimate the shear stress using a computational fluid dynamics approach [4].
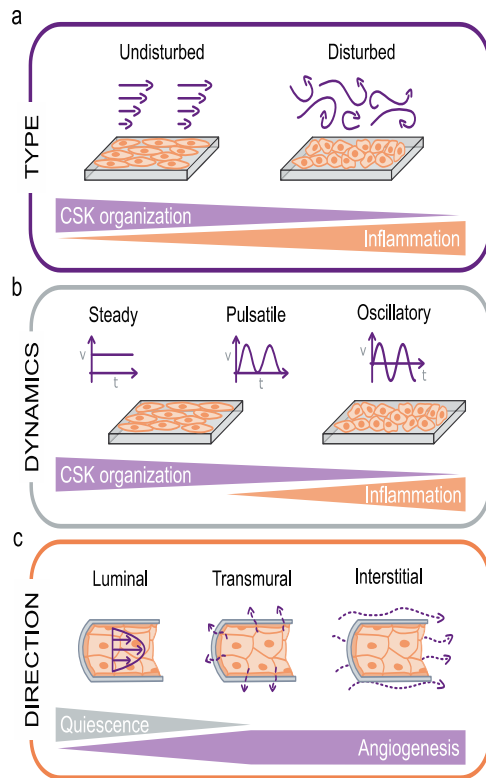
Figure (8): a) Shear stress and its impact on the vascular endothelial layer: The endothelial layer experiences either laminar or turbulent flows, each affecting the organization of cellular structures and the inflammatory state differently. b) Shear stress affects the endothelial layer under various flow conditions, including steady, pulsatile, or oscillatory flow patterns. These flow dynamics play a role in shaping the organization of cellular structures and the inflammatory state of the cells. c) The endothelial layer is exposed to different flow directions: luminal (along the cell surface), transmural (across cell-cell junctions), or interstitial (within the vessel wall or parenchymal tissue). The flow direction influences whether the endothelium remains inactive or undergoes angiogenesis [13] .

2.2 In vitro measurements

An in vitro arrangement offers a controlled environment for testing heart valves with good repeatability, and this can be achieved using a Pulse Duplicator System PDS. The PDS serves as a hydraulic simulation pertaining to the left side associated with the human heart, linked to a windkessel model that emulates the circulatory system [4]. Figure 9 provides a schematic illustration of the PDS device. The tested blood analogue composed of 47.6% by volume of glycerin solution in water at $36.5\pm0.5C^0$, which effectively simulates the dynamic viscosity of blood (4.0 mPa.s)[14]. These synthetic heart models serve as a means to evaluate various artificial heart valves, allowing for measurements of pressure, flow, and even Doppler assessments [4]. With the utilization of these setups, it becomes achievable to evaluate the hydrodynamic effectiveness of synthetic heart valves within a controlled outside of a living organism setting. In addition, in physiological

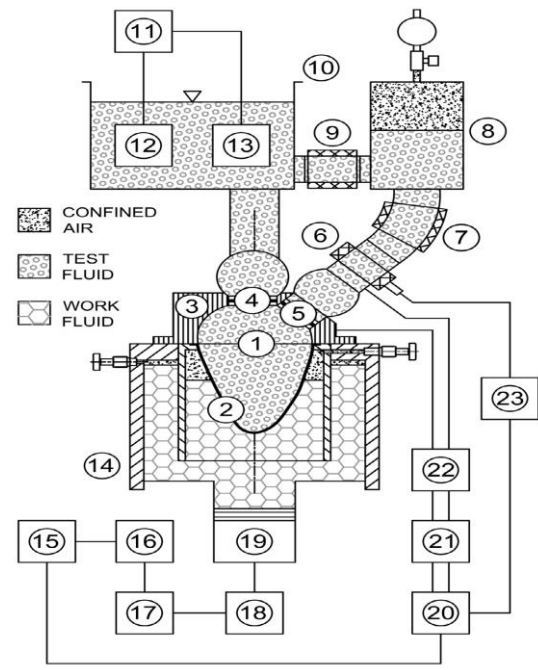and pathophysiological conditions, different level of valve stenosis can be simulated [20].

Figure (9): Diagram illustrating a pulse duplicator simulator configuration. The setup includes a model representing the left ventricle (1), a pliable membrane (2), an acrylic optical platform suitable for laser velocimetry applications (3), a valve mimicking the mitral valve (4), an aortic valve (5), a flow measurement probe (6), a component simulating characteristic resistance (7), adjustable compliance settings (8), customizable peripheral resistance (9), a reservoir preceding the atrium (10), a digital thermostat (11), a temperature sensor (12), a heating unit (13), a reservoir for the working fluid (14), a microcomputer for supervisory control and data acquisition (15), a drive system for a servomotor (16), the servomotor itself (17), a linear sliding mechanism (18), a hydraulic cylinder (19), a data acquisition (DAQ) module (20), signal conditioning units (21), invasive blood pressure transducers (22), and a flow measurement device (23)[14].

2.3 Animal experimental model

One of the prerequisites of developing a new cardiac valvular prosthesis is a successful pre-clinical large animal series. An appropriate animal model may provide information on valve performance, safety, and in vivo hemodynamics. However, no suitable animal model is available that can yield such information for a prosthetic aortic valve. Many animal models have been used with variable results. These include sheep, goats, dogs, pigs, calves and primates. Goats have been found to be a good model for valve testing, but their availability is often limited. The relative susceptibility of dogs to sepsis and thrombosis has marked these animals as less than optimal. Sheep (Ovis aris) are widely used for testing prosthetic cardiac valves. The pig is more advantageous in terms of cost and availability, but it too shares the limitations of cloven footed animals of having a short ascending aortic trunk, a tendency to develop cardiopulmonary bypass

complications, and presenting difficulties in terms of accessing the peripheral venous circulation, management and handling [15] . On other aspect, studies that dealing with genetic and epigenetic causes of heart malformations employ small animal models. Zebrafish and chicken embryos are well-suited. Mouse embryos offer advantage for genetic manipulations and lineage tracing studies [15] .

2.4 Computational model:

Computational modeling stands as an indispensable tool for probing the intricate mechanics of the aortic heart valve. Within this context, the heart valve environment showcases complex dynamics and mechanical behaviors, with solid structures interplaying within a fluid domain. Computational investigations of the aortic valve have yielded profound insights into understanding the mechanics of healthy valves, tracking the progression of diseased ones, and making predictions regarding the durability and effectiveness of surgical interventions and valve replacement .The absence of a universally accepted approach has led to the application of various strategies in tackling the diverse facets of heart valve modeling[16].

2.4.1. Fluid- structure interaction

Within the realm of Fluid-Structure Interaction (FSI), where the dynamics of blood affect the behavior of solid valve components, and vice versa, multiple models have been employed. Some models have concentrated solely on the structural aspects of aortic valve mechanics, while others have delved into the fluid dynamics associated with left ventricular ejection. However, modeling both valvular structures and a moving fluid volume simultaneously poses a non-trivial challenge[16].In these simulations, thin-walled leaflet structures undergo significant deformations within the fluid flow. Typically, fluid domains are represented using an Eulerian reference frame, where the mesh remains stationary regardless of fluid motion. In contrast, solid structures like leaflets or the root of the valve are modeled using a Lagrangian reference frame, where the mesh moves and deforms along with the structure. This movement of solid structures through the fluid introduces challenges to computational modeling techniques. Methods like the Arbitrary Lagrange-Euler (ALE) approach enable a deformable fluid mesh, while others like the operator splitting method or fictitious domain technique maintain a stationary fluid mesh. Although ALE is commonly used in FSI studies, it faces challenges in valve models. Managing the large movement of leaflet structures through the fluid mesh is better achieved by strategies employing a static fluid mesh[16]. Furthermore, commercial finite element method (FEM) software, such as LS-DYNA, has been employed to facilitate robust numerical methods for fluid-structure interaction. These software packages support complex geometries, including those derived from MRI data, and visualize flow patterns. Additionally, advancements have been made in simulating the progressive coaptation of leaflets, sealing against flow.FSI studies have demonstrated how blood flow through the valve is altered by the anatomical structures present, and how correspondingly the movement of blood instigates and participates in the opening and closing of the valve leaflets. These models which include the coupling of fluid and solid have already succeeded in examining the effects of root compliancy, assessing the importance of fiber-reinforcement in leaflet tissue [18], comparing different repair techniques, and investigating the congenital bicuspid valve.

Compared to solid-only models, fluid-structure interaction provides a more realistic and physiologically relevant simulation of valve function. Regardless of the specific method or technique employed for FSI, assumptions are generally made regarding the fluid phase, considering it as isothermal, incompressible, homogeneous, Newtonian, and laminar. Although blood exhibits non-Newtonian behavior, it can be approximated as Newtonian in regions with high shear rates and relatively large vessel diameters. Turbulent flow in the aortic valve region remains challenging to recreate computationally, limiting models to laminar flow until improved techniques become available[16].

2.4.2. Multi-scale approach

In the realm of leaflet tissue modeling, only a few models have managed to delineate the distinct layers of these vital components. These layers, known as the ventricularis, spongiosa, and fibrosa, each possess distinct material properties. However, a select few of these models, renowned for their precision in material characterization, incorporate fluid-structure interaction to more faithfully recreate the physiological context. One particularly noteworthy model, developed by Weinberg and Mofrad [17] in their seminal work, stands out. Not only does it meticulously describe the individual layers of valvular tissue using nonlinear anisotropic designations within a fluid domain, but it also exhibits the remarkable capability to simulate the organ, tissue, and cellular levels of the cardiovascular system. This multiscale approach enables a comprehensive analysis, ranging from the intricate interplay of structures and fluids at the organ level down to cellular deformations that signify a biological response [16]. In the Weinberg and Mofrad [17]. study, a set of reference configurations was established to characterize the tissue state, transitioning from individual layers to a fully loaded valve assembly. These reference configurations, originally devised by Stella and Sacks, provide a structural framework. The journey begins with configuration 0, where the fibrosa and ventricularis layers are separate and stress-free. These layers are then combined with the appropriate corrugations and arrangement to construct configuration 1. Subsequently, the tissue is assembled into the valve structure without pressure in configuration 2. Configuration 3 introduces physiological pressure to establish the initial state, and over time, 't' represents the functioning valve. Radial and circumferential extensibilities were meticulously assigned based on published experimental data for each configuration. The stretches required to transition between these configurations were computed using the extensibility data. These reference configurations serve as the foundation for multiscale simulations, where information flows seamlessly from

the organ to tissue and finally to the cellular level. The organ-scale simulations were executed using LS-DYNA (LSTC, Livermore, CA, USA), a reliable implicit commercial finite element program. For the tissue-level simulations, an implicit software, ADINA (ADINA R&D, Watertown, MA), was employed. At the cell scale, the model involved a single cell surrounded by matrix, meticulously analyzed within the framework of implicit ADINA software. This approach allowed for an in-depth exploration of the mechanical responses of individual tissue layers, taking into account the unique corrugated nature of the fibrous layers, (See Fig. 9 for visual representation) [16].
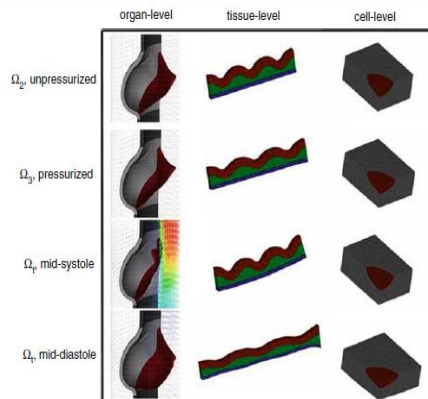
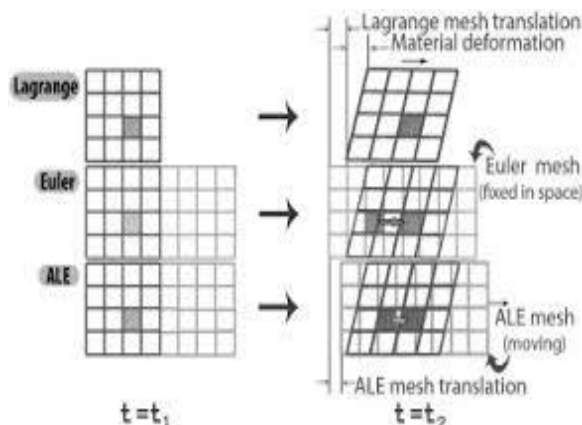**Figure(10):** Deformation observed within each of the three stages in the multi-scale model[16].

Figure (11): Lagrangian, Eulerian and ALE meshes and element Motion[18].

2.5 Imaging modality in prosthetic valve assessment.

Current imaging modalities include fluoroscopy, which is limited to the assessment of mechanical PHV leaflet motion, and echocardiography. Echocardiography is the mainstay for evaluation of PHV function providing both functional (Doppler) and anatomic information. However, echo-cardiograph may not identify the morphological cause of PHV dysfunction or provide information on its extent because of acoustic shadowing, complex anatomy, and limited viewing windows.

Computed tomography (CT) and magnetic resonance imaging (MRI) have established their role in cardiac imaging. Several, yet diverse studies have advocated.

MRI and more prominently CT as new imaging techniques for PHV assessment to complement echocardiography.

CT and MRI may provide incremental information in selected patients by uncoupling image analysis and acquisition and providing a complete anatomic overview. CT can identify morphological correlates of obstruction such as (peri) prosthetic masses, restricted leaflet motion, left ventricular outflow tract obstruction, and thickening and calcification of leaflets, which could be of importance for valve-in-valve procedures.

MRI allowed annular and orifice area measurements in biological valves with good agreement to echocardiography and assessment of flow and velocity pat- terns in biological mechanical valves. MRI may potentially demonstrate abnormal asymmetrical flow patterns in PHV obstruct although leaflet angle measurements may not be possible [19, 20].

2.6 Experimental visualization of blood flow in the sinus

Sinus flow characteristics exhibit a profound interplay with the intricate hemodynamic parameters that prevail within the sinus cavity .In a study conducted by Forleo et.al [21]. A novel in-vitro technique was introduced to quantitatively investigate the impact of vortex formation and regurgitated jet flow, situated proximate to the hinge region of a bileaflet mechanical aortic valve, on the Blood Damage Index (BDI). Their findings illuminated the consequential influence of mechanical valve replacement on BDI, manifesting as a notable reduction in valve closing time by 10 milliseconds and a concurrent elevation in mean aortic pressure by 40 mmHg. This heightened mean pressure engendered robust vortex structures, subsequently inciting platelet activation and a concomitant escalation in BDI [21].

In a parallel investigation conducted by Moore et al., their study unveiled the profound impact of various cardiac rhythms on the dynamics of leaflet flutter during systole. Intriguingly, they discerned complex spatiotemporal vortex structures within the sinuses, fostering a highly intricate milieu. To elucidate the hypothesis that calcification manifests earlier in the non-coronary sinus, a meticulous comparison of vortex structures was orchestrated between the coronary and non-coronary sinuses.

The subsequent investigation, as elucidated by Moore et al., elucidated that the presence of coronary blood flow exerts a modulating influence on leaflet dynamics, concurrently mitigating the wall shear stress experienced by the leaflets. However, this adjustment resulted in an improvement in washout time, denoting the temporal span required for blood to traverse from the sinuses to the base of the aorta. These multifaceted observations collectively contribute to our comprehension of the intricate interplay between sinus flow dynamics, valve design, and hemodynamic outcomes, thereby advancing our understanding of aortic valve pathophysiology and potential therapeutic strategies.

2.7. Findings obtained from both researches involving both real - world medical settings and controlled laboratory investigations of heart valve

These findings pertain to both clinical and experimental investigations regarding the hemodynamic characteristics of mechanical aortic valves. While these studies may be somewhat dated, their relevance remains integral in elucidating and achieving the objectives of our review.

2.7.1. Pressure gradient

The St. Jude Medical Hemodynamic Plus (SJM HP) and On-X valves exhibited the least average pressure drop in laboratory tests, figure12. Differences in these pressure drops were associated with the dimensions of the geometric opening and the extent of valve opening. Additionally, the SJM HP valve gains an advantage from its more spacious internal orifice diameter and a notable angle of valve opening. Additionally, as depicted in figure13, it becomes apparent that increasing cardiac output leading to more pronounced pressure drop. Within a clinical setting, it becomes impractical to non-invasively measure this peak pressure gradient due to the challenges in positioning a catheter across or between the leaflets of a mechanical prosthetic valve. Doppler gradients measured across the central openings display notably higher measurements when compared to the catheter pressure gradients across the valve, both transvalvular and net, as depicted in figure 14 due to the phenomenon of downstream pressure recovery (as depicted in figure 15). The pressure recovery phenomenon delineates pressure readings taken at specific intervals along the axis of the valve. Initially, there is a pressure drop, but this is followed by a subsequent rebound at a specific point further down the flow from the valve. This recovery because the kinetic energy of the flow transforms into potential energy as the flow decelerates while passing through the valve [4].
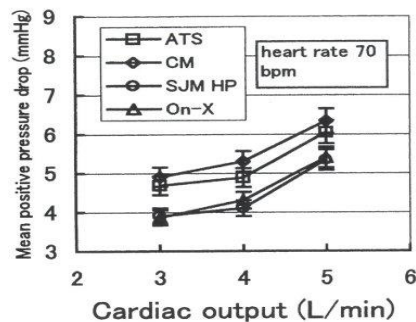

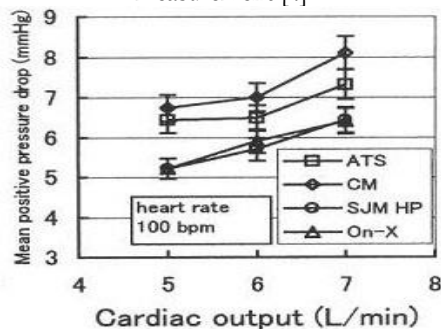**Figure (12):** Example of pressure gradient measurement [4].

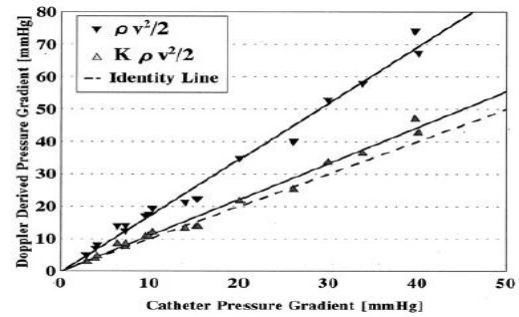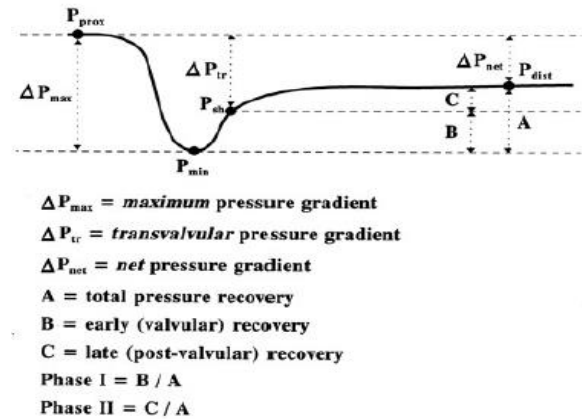**Figure (13):** Pressure gradient for different valves prostheses at HR 70 and 100.

Figure (14): Correlation between catheter transvalvular pressure gradients and Doppler-derived pressure gradients.

ΔP_{max} = maximum pressure gradient

ΔP_{tr} = transvalvular pressure gradient

ΔP_{net} = net pressure gradient

A = total pressure recovery

B = early (valvular) recovery

C = late (post-valvular) recovery

Phase I = B / A

Phase II = C / A

Figure(15): Schematic representation of a centerline pressure profile showing the locations where pressures were read out for comparison [4].

2.7.2. Effective orifice area

The EOA serves as the basis for calculating the Performance Index (PI), which offers a means to compare various kinds of heart valves. A higher PI indicates superior fluid dynamics characteristics of the examined valve, implying reduced flow constriction and efficient utilization of the existing opening's geometric area.

The EOA is not universal for all patient but it is individual i.e. patient dependent, however; it remains a useful factor for prosthetic valve selection and postoperative assessment in spite of its influentiality by patients left ventricular outflow anatomy [22].

Figure (10) describes the relationship between prosthetic valve size and EOA in vivo and in vitro [22][21]. In vivo, valve size could explain 31% and 37% (R^2) of the variability in calculated EOA in the SJM and OMNI valves, respectively. A wide dis-tribution was present, with the coefficient of variation (SD/mean × 100%) ranging from 21% to 39% for the SJM valve and from 25% to 33% for the OMNI valve. In vitro, valve size could explain 97% of the variability in EOA in both the SJM and OMNI valves. We observed a very narrow dis- tribution, with coefficients of variation ranging from 1% to 7% in the SJM valve and from 1% to 5% in the OMNI valve. The discrepancies between geometric orifice valve areas and EOAPeak were 0.96 ± 0.49 cm2 for SJM versus 0.87 ± 0.59 cm2 for OMNI valves in vivo and 1.26 ± 0.41 cm2 for SJM versus 1.17 ± 0.38 cm2 for OMNI valves in vitro [23].
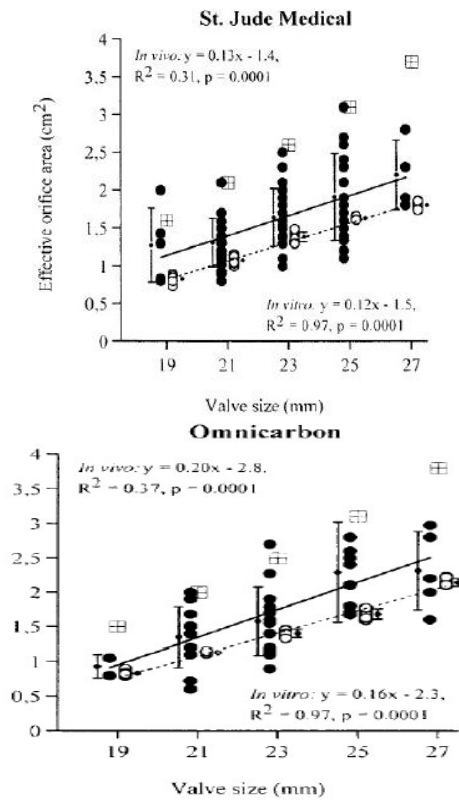
Figure (16): The effective orifice area is compared between two distinct mechanical valve categories. The outcomes are displayed for both in vivo (depicted as black circles) and in vitro (represented by open circles) investigations. The bars signify the mean value along with the standard deviation (SD). The area of the geometric opening is depicted through the boxes[4].

2.7.3. Regurgitation

Figure 17 provides an instance of data concerning regurgitation in various categories of bi-leaflet valves [24]. The closing volume, expressed as a percentage of the forward flow volume, grew larger as the cardiac output decreased. The closing volumes shown in figure 17 for the valves remain within the acceptable threshold (<8%). During the low cardiac output scenario at a rate of 100 beats per minute, the SJM HP valve displayed a slightly higher closing volume of 11.4% [4].

The connection between the closing volume and the angle of opening of the mechanical heart valve as depicted in figures 17(a) and (b)) is believed to be directly proportional. Clearly, the SJM HP valve displays the broadest angle of opening and uniformly maintains the highest closing volume across all operational scenarios. In contrast, the CM and ATS valves, with their narrower opening angles, result in smaller closing volumes. Despite its parallel-opening leaflet design (angle of 90), the On-X valve has low closing volume. The reason for that is the actual non-fully open and the original small travel angle design minimizes the volume that is swept during closure. Consequently, the On-X valve typically exhibits a closing volume similar to that of the CM valve [4].
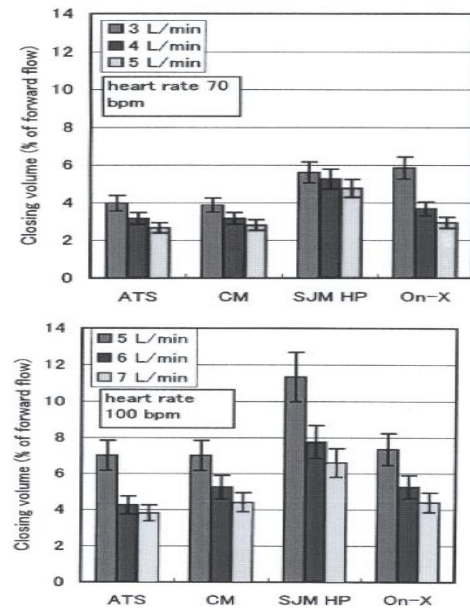

Figure (17): Various bi-leaflet heart valves closing volume (ATS: Advancing The Standard, CM: Carbomedics, SJM HP: St. Jude Medical Hemodynamic Plus, On-X) using an experimental arrangement that simulated the mitral position. This study was conducted at both 70 beats per minute and 100 beats per minute [4].

2.7.4. Patterns of fluid flow and stresses exerted by shear force

Bi-leaflet valves offer the most accurate representation of central flow observed in a mechanical heart valve (figure18, c). Presence of 2-leaflets restricts the flow to a certain degree, resulting in a three-component flow configuration. As a consequence, elevated turbulent shear stresses are detected at positions directly downstream from the valve leaflets (figure 19, c)[4].
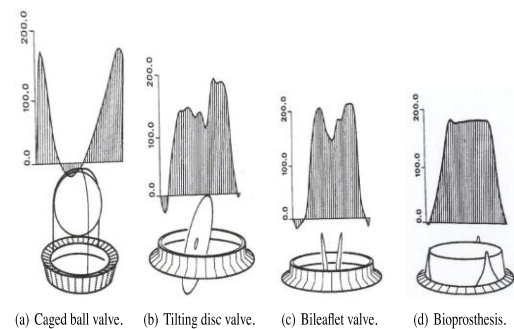

(a) Caged ball valve.   (b) Tilting disc valve.   (c) Bileaflet valve.   (d) Bioprosthesis.

Figure (18): Velocity profile based on in vitro measurements on 27 mm aortic valve designs.

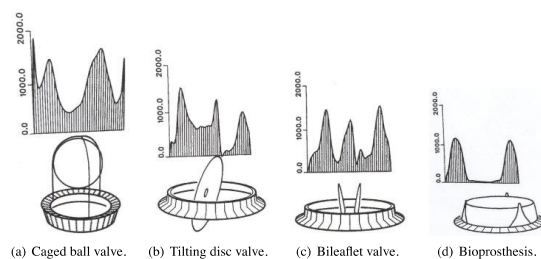(a) Caged ball valve.   (b) Tilting disc valve.   (c) Bileaflet valve.   (d) Bioprosthesis.

Figure (19): Turbulent shear stress in 0.1 N/m^2 profiles measured in vitro experiments in 27 mm aortic valve configurations [4].

3. Conclusion

In summary, this introductory article has provided a foundational overview of the intricate subject of assessing aortic valve prosthesis. Though a comprehensive examination of relevant literatures and methodologies, we have laid the groundwork for further research and exploration in this complex field. By elucidating the key considerations and methodologies involved in the evaluation of aortic valve prosthetic devices, we hope to pave the way for more in-depth studies and advancements in this critical area of cardiac research. the primary objective of this comprehensive review is to elucidate, with utmost precision, the multifaceted methodologies employed in the investigation and evaluation of mechanical prosthetic aortic valve. As we continue to delve deeper into this subject, we anticipated that future research will build upon the framework presented here.

4. References

[1] Seoudy, H., *Limitations of echocardiography in the assessment of aortic valve disease.* Journal of Cardiology Practice, 2020. **18**: p. 17-28.

[2] Bokros, J., *Monoleaflet Tilting Disc Valves*, in *Heart of Carbon: The Story Behind the Pursuit of the Perfect Mechanical Heart Valve*. 2023, Springer. p. 53-66.

[3] Ciolacu, D.E., R. Nicu, and F. Ciolacu, *Natural polymers in heart valve tissue engineering: Strategies, advances and challenges.* Biomedicines, 2022. **10**(5): p. 1095.

[4] Dumont, K., *Experimental and numerical modeling of heart valve dynamics.* 2004, Ghent University.

[5] Angellotti, D., et al., *Is There Still a Role for Invasive Assessment of Aortic Gradient?* Diagnostics, 2023. **13**(10): p. 1698.

[6] Hatoum, H., et al., *Modeling of the instantaneous transvalvular pressure gradient in aortic stenosis.* Annals of biomedical engineering, 2019. **47**: p. 1748-1763.

[7] Baumgartner, H., et al., *Recommendations on the echocardiographic assessment of aortic valve stenosis: a focused update from the European Association of Cardiovascular Imaging and the American Society of Echocardiography.* European Heart Journal-Cardiovascular Imaging, 2017. **18**(3): p. 254-275.

[8] Caballero, A., et al., *New insights into mitral heart valve prolapse after chordae rupture through fluid–structure interaction computational modeling.* Scientific reports, 2018. **8**(1): p. 17306.

[9] Abd Malek, A.F., *Evaluation of Granular Fertilizer Boom Sprayer Performance Via Computational Simulation.* 2015, Universiti Tun Hussein Onn Malaysia.

[10] Welty, J., G.L. Rorrer, and D.G. Foster, *Fundamentals of momentum, heat, and mass transfer.* 2020: John Wiley & Sons.

[11] Roux, E., et al., *Fluid shear stress sensing by the endothelial layer.* Frontiers in Physiology, 2020. **11**: p. 861.

[12] Heil, M. and W. Schaper, *Influence of mechanical, cellular, and molecular factors on collateral artery growth (arteriogenesis).* Circulation research, 2004. **95**(5): p. 449-458.

[13] Dessalles, C.A., et al., *Integration of substrate- and flow-derived stresses in endothelial cell mechanobiology.* Communications Biology, 2021. **4**(1): p. 764.

[14] Bazan, O. and J.P. Ortiz, *Experimental validation of a cardiac simulator for in vitro evaluation of prosthetic heart valves.* Brazilian Journal of Cardiovascular Surgery, 2016. **31**: p. 151-157.

[15] Kheradvar, A., et al., *Animal models for heart valve research and development.* Drug Discovery Today: Disease Models, 2017. **24**: p. 55-62.

[16] Croft, L.R. and M.R.K. Mofrad, *Computational modeling of aortic heart valves.* Computational Modeling in Biomechanics, 2010: p. 221-252.

[17] Weinberg, E.J., D. Shahmirzadi, and M.R.K. Mofrad, *On the multiscale modeling of heart valve biomechanics in health and disease.* Biomechanics and modeling in mechanobiology, 2010. **9**: p. 373-387.

[18] Mobaraki, B. and M. Vaghefi, *Numerical study of the depth and cross-sectional shape of tunnel under surface explosion.* Tunnelling and underground space technology, 2015. **47**: p. 114-122.

[19] Rajiah, P., et al., *Multimodality imaging of complications of cardiac valve surgeries.* Radiographics, 2019. **39**(4): p. 932-956.

[20] Sucha, D., et al., *Multimodality imaging assessment of prosthetic heart valves.* Circulation: Cardiovascular Imaging, 2015. **8**(9): p. e003703.

[21] Forleo, M. and L.P. Dasi, *Effect of hypertension on the closing dynamics and lagrangian blood damage index measure of the B-Datum Regurgitant Jet in a bileaflet mechanical heart valve.* Annals of biomedical engineering, 2014. **42**: p. 110-122.

[22] Elefteriades, J.A. and B.A. Ziganshin, *Reply: Effective orifice area of prosthetic heart valves—not perfect, but still valuable.* The Journal of Thoracic and Cardiovascular Surgery, 2020. **159**(6): p. e330-e332.

[23] Bech-Hanssen, O., et al., *Assessment of effective orifice area of prosthetic aortic valves with Doppler echocardiography: an in vivo and in vitro study.* The Journal of thoracic and cardiovascular surgery, 2001. **122**(2): p. 287-295.

[24] Feng, Z., et al., *In vitro investigation of opening behavior and hydrodynamics of bileaflet valves in the mitral position.* Artificial organs, 2002. **26**(1): p. 32-39.